On the use of Boundary Conditions and Thermophysical properties of Nanoparticles for application of Nanofluids as coolant in Nuclear Power Plants; A Numerical Study

Hamidreza Arab Bafrani[a], Omid Noori-kalkhoran[b,1], Massimiliano Gei[b], Rohollah Ahangari[c], Mohammad Mahdi Mirzaee[a]

[a]Faculty of Engineering, Shahid Beheshti University, Tehran, Iran

[b]School of Engineering, Cardiff University, The Parade, Cardiff CF24 3AA, Wales, UK

[c]Safety and Reactor School,Nuclear Science and Technology Research Institute, Tehran, Iran

Number of manuscript pages: 37

Number of Figures: 20

Number of Tables:11

[1] Corresponding Author Email address: NoorikalkhoranO@Cardiff.ac.uk

Abstract:

In the first part of the present study, a thermal-hydraulic subchannel code hereafter called 'SUBTHAC' is developed to evaluate the enhancement effects of nanoparticles in core heat transfer. The first version of SUBTHAC (V1.0) can analyze the steady state flow of coolant with Al_2O_3, TiO_2 or CuO as nanoparticles (other types of nanoparticles can be added by the user). Different output profiles can be selected such as fluid temperature, pressure and velocity for each subchannel, clad outside temperature for each fuel rod, axial and lateral mass flow, etc. SUBTHAC uses a dedicated algorithm to solve the subchannel equations and, unlike many other codes, allows for thermophysical parameters of nanoparticles to be a function of the *temperature,* leading to improvement the accuracy of results. Results computed by SUBTHAC for base fluid (pure water) are validated against those obtained by COBRA-EN code. In the next step, with the aim of validating the capability of nanofluid analysis of SUBTHAC code, its nanofluids results have been validated against reference CFD simulations. After the validation, comprehensive numerical comparisons are conducted to assess the enhancement of thermal-hydraulic parameters by using nanofluids. It is shown that, among Al_2O_3, TiO_2 and CuO nanofluids with volumetric concentration in the range of 1-5%, TiO_2-3% and CuO-3% are the best choices to increase fluid outlet temperature and decrease clad temperature, respectively. Using nanofluids with a concentration higher than 3% volumetric is not justifiable as the core pressure drop increases up to more than 20%.

In the second part of the manuscript, some relevant remarks are put forward on the assignment of boundary conditions (BC, i.e. inlet velocity/inlet mass flux/inlet Reynolds number) and the adoption of reliable values for specific heat capacity of nanoparticles *in operational temperature of NPPs*. The effects of using the above boundary conditions and incorrect values of the specific heat (as adopted in the literature so far) are depicted by presenting some profiles of coolant and clad temperature. Selecting different BCs and incorrect values of specific heat for nanoparticles can jeopardize the results of calculations.

Keywords: Nanofluid; Heat transfer enhancement; Subchannel analysis; Nuclear Thermal-hydraulic code, Specific heat capacity; Boundary conditions

Nomenclature

Symbol	Unit	Definition
A	[m^2]	Area
Cp	[J/kgK]	Specific heat
D	[m]	Diameter
f_w	[-]	Friction factor
g	[m/s^2]	Acceleration due to gravity
h	[J/kg]	Enthalpy
h_{con}	[W/m^2K]	Heat transfer coefficient
K	[W/m K]	Thermal conductivity
k_G	[-]	Both friction and form drag factor
l	[m]	Centroid distance
Nu	[-]	Nusselt number
P	[Pa]	Pressure
p	[m]	Perimeter
Pr	[-]	Prandtl number
q''	[W/m^2]	Heat flux
Re	[-]	Reynolds number
s	[m]	Width of the gap
T	[K]	Temperature
t	[s]	Time
u	[m/s]	Velocity
w	[kg/m s]	Mass flow per unit length in the lateral direction through the gap
w'	[kg/m s]	Turbulent mixing flow rate per unit length through the gap
z	[m]	Axial direction
C_T	[-]	Modelling parameter (is equal to zero in this article)
Greek symbols		
ρ	[kg/m^3]	Density
μ	[Pa s]	Viscosity
ϕ	[-]	Nanoparticle volume fraction
ψ	[-]	Correction factor for the Nusselt number
β	[-]	The ratio of the nano layer thickness to the original particle radius
Subscripts and superscript		
i,j,k		Node and subchannel‘s index
bf		Base fluid
h		Heated
hy		Hydraulic
nf		Nanofluid
np		Nanoparticle
w		Wetted
$clad$		Clad outside surface
$c.t.$		Circular tube
*		Donor cell parameter

1. Introduction

A *nanofluid* is a colloidal dispersion of nanoparticles in a base fluid such as water, engine oil, Ethylene Glycol, etc. Due to the addition of nanoparticles to the base fluid, the properties of nanofluids, including thermo-physical ones, differ in comparison with those of the base fluid alone. Depending on the type of application, these differences may play either a positive or a negative role. One of the most important positive differences is modification of the thermal conductivity of nanofluids that may lead to an improvement in the heat removal, suggesting the possibility of using nanofluids as coolant in nuclear reactors, i.e., primary coolant, safety systems and severe accident mitigation strategies [1].

Pressurized water reactors (PWRs) are the most common nuclear reactors all around the world. In this type of reactor, pressurized light water (at a pressure of about 16 MPa) is used as a coolant. On the one hand, adding nanoparticles to water can enhance the Critical Heat Flux (CHF) limits and accelerate quenching heat in the reactor core. These features can be exploited in PWR to realize sizable power up rates in the core, thus attaining either significant economic gains or improved safety margins [2]. On the other hand, it should be considered that adding nanoparticles to NPPs' coolant can increase the pressure drop in the core (needing more pump power), enhance the risk of deposition of nanoparticles in fluid channels (favouring their blockage) and make nanoparticles as new radioactive sources. Therefore, finding a balance between the heat transfer modification of nanoparticles and their above-mentioned drawbacks is vital for the practical use of nanofluids in NPPs.

There are two models for the thermohydraulic analysis of nanofluid flow [3]:

1) homogeneous flow model: the velocities of base fluid and nanoparticles are assumed to be equal and the volume concentration of the nanoparticle is considered constant all over the domain;
2) dispersion model: there is a slip velocity between base fluid and nanoparticles and the volumetric concentration of the latter can vary spatially in the domain.

Due to the importance of heat transfer enhancement in NPPs and the attractive properties of nanofluids, different scientists and research groups are working in this field to predict the effect of nanoparticles on base fluid behaviour and assess their employment in NPPs. Most of their studies are based on numerical simulations (by developing in-house codes or using available CFD software) while some others are using thermal-hydraulic loops to estimate experimentally

the benefit of nanoparticles. Concerning another categorization, some papers investigated only thermal-hydraulic effects of nanoparticles, whereas others also focused on the neutronic outcome (i.e. effects of nanoparticles on neutronic parameters of cores) that is very important in the assessment of criticality of the reactor core.

Part of those studies dealt with the review of nanofluid properties especially those related to the heat transfer process. A complete review of thermal conductivity models for nanofluids was conducted by Aybar et al. [4] who discussed different mechanisms of enhancement nanofluids' thermal conductivity. Meyer et al. reviewed theoretical, empirical and numerical models of the viscosity properties of nanofluids [5]. Heat transfer characteristics in nanofluid have been reviewed in [6] where it is addressed convective heat transfer performance, thermophysical properties, effect of fluid temperature and the change of some other physical parameters. Another review, conducted by Kumar Das et al [7] dealt with heat transfer in nanofluid with focus on other modes of heat transfer (other than conductivity like radiation) to develop a comprehensive theory of heat transfer in nanofluids.

Evaluation of nanofluid and nanoparticle effects on thermal-hydraulic profiles of nuclear power plants forms another important field of investigation. A numerical analysis of the water-Al_2O_3 nanofluid turbulent forced convection in VVER-1000 nuclear reactor was performed by Hadad et al [8]. They reported that either injection of the nanoparticle to the core or increase its volume fraction would raise the channel outlet temperature. In another study [9], the role of nanofluid as coolant, neutron absorber and moderator at the same time was investigated in a VVER-1000 NPP. Zarifi et al. studied the thermohydraulic analysis of Al_2O_3 and TiO_2 nanofluids as coolant in VVER-1000 reactor [10]. They reported that no significant differences in thermohydraulic behaviour of Al_2O_3 and TiO_2 nanofluids were observed in their work. Similar studies [11–14] reached a similar conclusion attained with different methods. These methods of solution included computational fluid dynamics, subchannel, single heated channel and porous media approaches. Numerous experimental and theoretical works have been performed by Prof Meyer and his research group [15–19]. Most of these studies include experimental investigations of nanofluid heat transfer in different geometries, convective heat transfer coefficient of nanofluids and effect of nanofluids in heat removal and pressure drop in channels.

In the first part of this paper, SUBTHAC nuclear code (based on the homogeneous flow model) is developed for thermal-hydraulic analysis of nanofluids in NPPs reactor core. The first version of the code (V1.0) can calculate the parameters in the steady-state situation (in

subsequent versions, transient calculations and two-phase model will be added as an additional module). In this version, Al_2O_3, TiO_2 and CuO nanoparticles (whose thermophysical parameters are considered as a function of temperature) with optional concentration can be selected and the resulted nanofluid is used as a coolant to calculate the thermal-hydraulic parameters of the reactor core. Custom nanoparticles can also be added to the relevant module by including their characteristic parameters as an input. The subchannel approach is employed to analyze the nanofluid flow in the core region. The code can automatically recognize and build subchannels by processing the input data. The proposed method and core algorithm enable the user to obtain some extra detailed information from the nanofluid analysis such as mass, momentum and energy transverse exchange which have not been reported in previous works. Figure 1 shows the SUBTHAC code structure and its submodules.

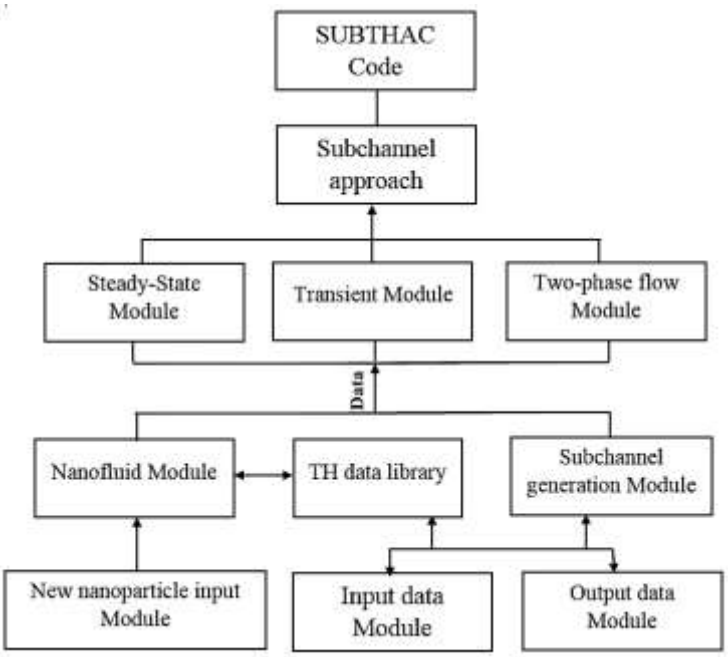

Figure 1. SUBTHAC code structure and modules.

One of the main challenges in the evaluation of nanofluid effects on heat transfer of NPPs is related to the selection of the correct Boundary Conditions (BCs) for fluid flow (among inlet velocity/inlet mass flux/inlet Reynolds number) -that should be equal with the base fluid one for a meaningful comparison of results- and the adoption of accurate values of specific heat capacity of the nanoparticles, the latter usually assumed as independent of the temperature. As shown in section 4, these two set of assumptions can affect strongly the results (and in some case can damage the philosophy of using nanoparticles) as they have opposite effects on outlet flow temperature and fuel structure (clad and fuel) temperature. Comprehensive numerical

investigations are then presented in section 4 to appraise to which extent these issues are important for a correct assessment of the use of nanofluids in NPPs.

2. Governing equations

The subchannel approach philosophy is based on dividing the fluid domain to individual channels that are connected together (Figure 2). One of the main assumptions is that there is no direction for lateral flow after leaving a gap between two channels. This assumption can eliminate the limitations about the connection of the subchannels together and as a result, it is possible to model a three-dimensional geometry by connecting the channels in a three-dimensional array. This leads to simplifications in the lateral convective terms of the linear momentum balance equation, allowing readily for axial flow situations. The use of such a procedure reduces the Navier-Stokes equations to a set of one-dimensional equations (the reader is referred to [20] for more details).

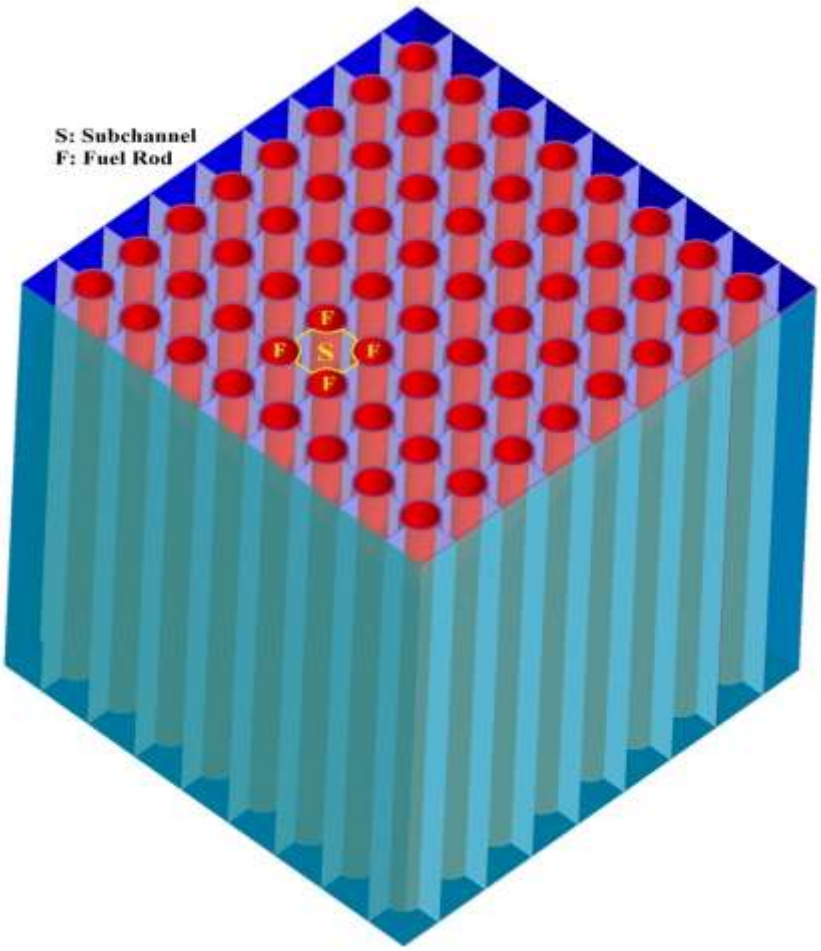

Figure 2. Overview of Subchannel approach geometry

To derive the subchannel equations, the integral balances for one-dimensional Navier-Stokes equations are imposed to a typical subchannel control volume. Furthermore, some empirical correlations are used to manipulate the set of equations. Eventually, the numerical results are obtained by applying finite-difference approximation. In this study, an implicit iterative algorithm called “Crossflow scheme” has been implemented for calculations. In this scheme, all equations (mass, energy, axial and lateral momentum) are solved separately and sequentially, node by node. Collocated meshes for mass, energy and axial momentum conservation equations and staggered ones for lateral momentum balance equations have been used in the solution.

2.1. Subchannel Analysis

Subchannel equations include: mass conservation, axial momentum balances, lateral momentum balance and energy equation. A typical subchannel control volume is shown in Figure 3.

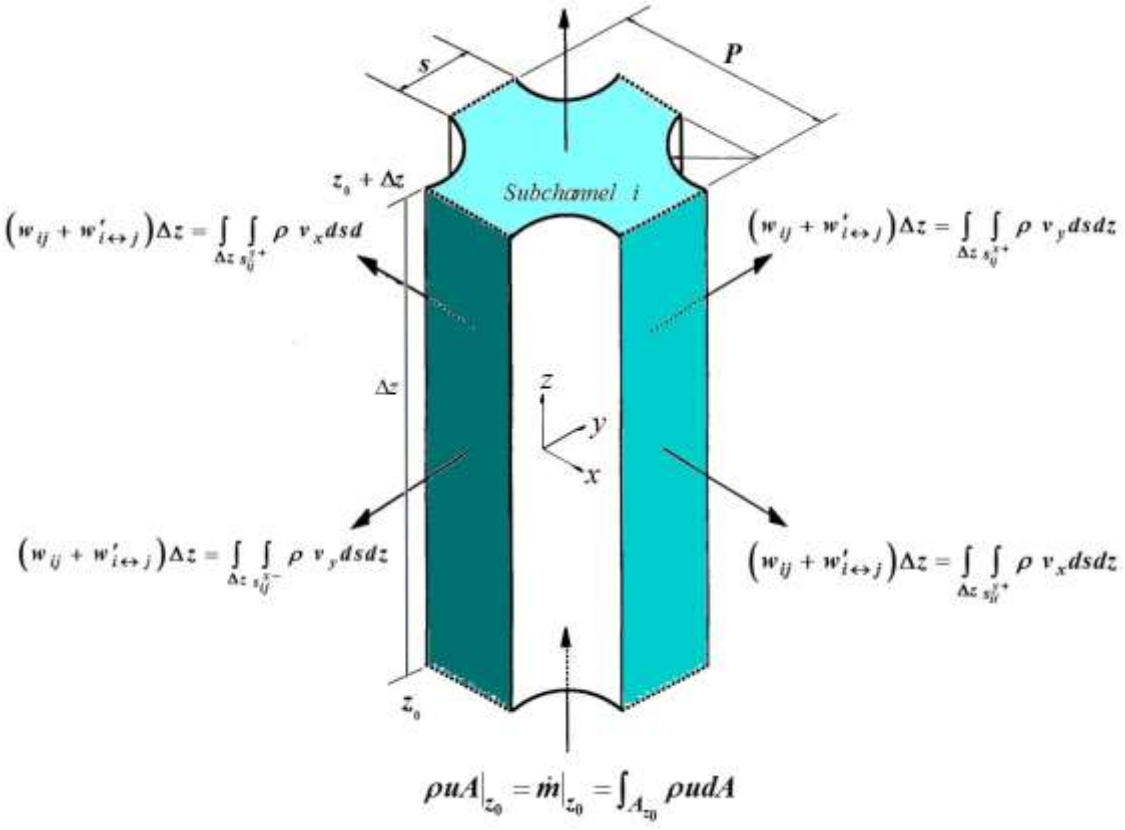

Figure 3. A typical subchannel control volume and its relevant equations.

2.1.1 Subchannel Mass Conservation Equation

For the single-phase flow, the continuity equation can be written as follows [20]:

$$A\frac{\partial \rho_{nf}}{\partial t} + \frac{\partial(\rho_{nf} uA)}{\partial z} + \sum w_{ij} + \sum w'_{i\leftrightarrow j} = 0, \qquad (1)$$

where u is the velocity in the axial primary direction, ρ_{nf} the nanofluid density, w' the turbulent mixing flow rate per unit length and w_{ij} is the mass flow per unit length in the lateral direction through the gap between the adjacent channels i and j.

The density of a nanofluid can be calculated by using the Pak and Cho correlations [21], which is defined by

$$\rho_{nf} = \phi\rho_{np} + (1-\phi)\rho_{bf}, \qquad (2)$$

where ϕ is the particle's volume fraction, ρ_{bf} is the density of the base fluid and ρ_{np} is the density of the nanoparticle. Table 1 shows the values of densities for base fluid and nanofluids that have been used in SUBTHAC.

Table 1. Densities (kg/m^3) of nanofluids (at 291 ^{o}C)

Nanoparticle	Concentration of nanoparticle		
	1 %	3 %	5 %
Al_2O_3	776.4966	841.0118	905.5271
TiO_2	775.7966	838.9118	902.0271
CuO	800.7966	913.9118	1027.027
Base fluid (Pure water)	744.239		

Here it has been considered that nanoparticle and base fluid are at the same velocity (homogeneous model). Therefore, the volume fraction of nanoparticles in the base fluid through the core remains constant and equals to the inlet value. Applied turbulent mixing model is based on the equal mass exchange between adjacent subchannels without any accumulation. Consequently, the fourth term in the right side of equation (1) (i.e., $\sum w'_{i\leftrightarrow j}$) is equal to zero.

2.1.2. Subchannel Axial Momentum Balance Equation

For the single-phase flow, the axial momentum balance equation for the i-th channel can be written as [20]

$$A\frac{\partial(\rho_{nf}u)}{\partial t}+\frac{\partial(\rho_{nf}u^2A)}{\partial z}+\sum w_{ij}u^*=-A\frac{\partial P}{\partial z}-\frac{1}{2}\left(\frac{f_w}{D_{hy}}+k_{ll}\right)\rho_{nf}u|u|A-C_T\sum w'(\Delta u)-A\rho_{nf}g, \quad (3)$$

and

$$u^*=\frac{1}{2}(u_i+u_j), \quad (4)$$

where f_w stands for friction factor and represents the wall shear stress due to the flow and the local loss coefficient and k_{ll} represents the effects of local changes in the flow channel geometry or area i.e., grid spacers. Due to the absence of the grid spacers in this study, the channel flow area is constant and therefore k_{ll} is zero.

The friction factor for the rod bundle is calculated through the Cheng and Todreas correlation [22]:

$$f_w=\frac{C_{fil}}{(Re_{nf})^{0.18}} \quad (5)$$

and

$$C_{fil}=a+b_1\left(\frac{pitch}{D_{rod}}-1\right)+b_2\left(\frac{pitch}{D_{rod}}-1\right)^2, \quad (6)$$

where the coefficients a, b_1, and b_2 for subchannels of hexagonal and square arrays are listed in [23]. Reynolds number of the nanofluid, Re_{nf}, is defined as

$$Re_{nf}=\frac{\rho_{nf}uD_{hy}}{\mu_{nf}}, \quad (7)$$

where D_{hy} is the hydraulic diameter and μ_{nf} is the nanofluid viscosity which, according to Batchelor correlation [21], takes the form

$$\mu_{nf}=\mu_{bf}(1+2.5\phi+6.5\phi^2). \quad (8)$$

The hydraulic diameter for each type of subchannel can be obtained from

$$D_{hy}=\frac{4A_{channel}}{p_w}, \quad (9)$$

where p_w is the wetted perimeter of the subchannel.

2.1.3. Subchannel Lateral Momentum Balance Equation

Due to the changes in pressure between adjacent subchannels through the gap, there is a cross-flow between them that can be modelled by the lateral momentum balance equation as

$$\frac{\partial w}{\partial t} + \frac{\partial (wu)}{\partial z} = \frac{s}{l}[P_{l+\Delta l} - P_l] - \frac{1}{2}\frac{s}{l} k_G \frac{w|\,w|}{\rho^*_{nf} s^2}, \qquad (10)$$

where ρ^*_{nf} is the nanofluid density in the donor cell and k_G is the loss coefficient for both friction and form drag caused by the area change, a parameter taken equal to 0.5 [20].

2.1.4. Subchannel Energy Conservation Equation

The subchannel energy conservation equation is given by [20]

$$A\frac{\partial (\rho_{nf} h_{nf})}{\partial t} + A\frac{\partial (\rho_{nf} u h_{nf})}{\partial z} + \sum w\, h^*_{nf} = \sum p_h q''_w - \sum w'\left(\Delta h_{nf}\right). \qquad (11)$$

To use the energy equation for the nanofluid analysis, some changes are to be made in equation (11). First, the nanofluid enthalpy gradient is changed as follows:

$$\partial h_{nf} = Cp_{nf}\partial T, \qquad (12)$$

where Cp_{nf} is the specific heat of nanofluid that can be written as [24]

$$Cp_{nf} = \frac{\phi\, Cp_{np}\rho_{np} + (1-\phi) Cp_{bf}\rho_{bf}}{\rho_{nf}}. \qquad (13)$$

Cp_{np} is the specific heat of the considered nanoparticle. For default nanoparticles of the code, the specific heat is indicated in Table 2 [25]. This quantity is functions of the temperature and increases up to 40% moving from room temperature (25 ºC) to reactor operation temperature (320 ºC). This variation can significantly affect the efficiency of the nanofluid and alter the results of the calculations. This important issue seemed not to have been properly addressed in the literature, as highlighted in the following Section 4 of this article.

Table 2. Specific heat of nanoparticles (Cp_{np}) [25]

Temperature [°C]	Cp [kJ/kg K]		
	Al_2O_3	TiO_2	CuO
25	0.811377	0.691936	0.531093
26.85	0.815496	0.694440	0.532576
126.85	0.986669	0.796119	0.588419
226.85	1.089825	0.853105	0.619282
326.85	1.155684	0.887470	0.640326

To exert the lateral turbulent energy exchanges term between channels, the nanofluid enthalpy is expressed as

$$h_{nf} = \frac{\phi h_{np}\rho_{np} + (1-\phi)h_{bf}\rho_{bf}}{\rho_{nf}}, \tag{14}$$

where the nanoparticle enthalpy h_{np} is defined as

$$h_{np} = \overline{Cp_{np}}T, \tag{15}$$

and

$$\overline{Cp_{np}(T)} = \frac{\int_0^T Cp_{np}(T)dT}{\int_0^T dT}. \tag{16}$$

By substituting equations (13), (14) and (15) into the energy conservation equation (11), the subchannel energy equation can be reformulated as

$$A\frac{\partial}{\partial t}\left(\phi\overline{Cp_{np}}T\rho_{np} + (1-\phi)h_{bf}\rho_{bf}\right) + \overline{\rho_{nf}u}ACp_{nf}\frac{\partial T}{\partial z} + \sum wh_{nf}^{*} = \sum p_H q_w'' - \sum w'\left(\Delta h_{nf}\right), \tag{17}$$

in which the quantity $\overline{\rho_{nf}u}$ for node k can be defined as

$$\overline{\rho_{nf}u} = \frac{1}{2}\left(\left(\rho_{nf}u\right)_k + \left(\rho_{nf}u\right)_{k-1}\right). \tag{18}$$

The turbulent mixing flow rate per unit length through the gap k between adjacent channels i and j is defined as follows [26]:

$$w'_{i\leftrightarrow j} = 0.0296\left(\frac{Re_i + Re_j}{2}\right)^{-0.1}\left(\frac{s_k}{l_k}\right)\left(\frac{D_i + D_j}{2}\right)\left(\frac{\rho_i u_i + \rho_j u_j}{2}\right). \tag{19}$$

2.2. Convective Heat Transfer

The use of nanofluids in nuclear reactors is motivated by the desire to enhance the thermal conductivity of the coolant that reveals itself in the temperature of the fuel elements. A typical fuel rod is made up of fuel, gap and clad. To calculate the temperature of clad outside in each axial level, which is in direct contact with the nanofluid, the convection heat transfer equation in the clad surface can be written as:

$$T_{\text{clad}} = T_{nf} + \frac{q''}{h_{con}}, \tag{20}$$

where h_{con} is the convection heat transfer coefficient and is defined by

$$h_{con} = \frac{Nu_{nf} K_{nf}}{D_{hy}}, \tag{21}$$

in which K_{nf} is the nanofluid thermal conductivity and Nu_{nf} the Nusselt number of the nanofluid. The thermal conductivity of the nanofluid was calculated though Yu and Choi correlation [27], as follows:

$$K_{nf} = \left[\frac{K_{np}+2K_{bf}+2(K_{np}+K_{bf})(1+\beta)^3\phi}{K_{np}+2K_{bf}+(K_{np}-K_{bf})(1+\beta)^3\phi}\right] K_{bf}, \tag{22}$$

where K_{np} is the thermal conductivity of the nanoparticles [25] (Table 3) and β is the ratio of the thickness of the nano layer to the original particle radius. Normally, the value of 0.1 is considered for β to calculate the thermal conductivity of the nanofluids [27].

Table 3. Thermo-physical properties of nanoparticles (K_{np} at 300 °C) [25]

Parameter	Al_2O_3	TiO_2	CuO
ρ_{nf} [kg/m^3]	3970	3900	6400
K_{np} [W/m K]	20.06	5.3	32.9

The Nusselt number of the nanofluid corresponds to

$$Nu_{nf} = \psi\left(Nu_{nf}\right)_{c.t.}, \tag{23}$$

where ψ is the correction factor for rod bundle configurations, expressed by Markoczy correlation [28] as

$$\psi = 1 + 0.912\,\mathrm{Re}_{nf}^{\,-0.1}\,\mathrm{Pr}_{nf}^{\,0.4}\left(1 - 2.0043e^{-\frac{D_{hy}}{D_{rod}}}\right). \tag{24}$$

$\left(Nu_{nf}\right)_{c.t.}$ is the local Nusselt number in a smooth circular tube given by the Gnielinsky equation [29]

$$\left(Nu_{nf}\right)_{c.t.} = \frac{\left(\frac{f_w}{8}\right)\left(\mathrm{Re}_{nf} - 1000\right)\mathrm{Pr}_{nf}}{1 + 12.7\sqrt{\frac{f_w}{8}}\left(\mathrm{Pr}_{nf}^{2/3} - 1\right)}. \qquad (25)$$

Finally, the Prandtl number, Pr_{nf}, is defined by

$$Pr_{nf} = \frac{\mu_{nf} Cp_{nf}}{K_{nf}}. \qquad (26)$$

2.3. Thermo-physical Properties of Nanoparticles

Accurate determination of nanoparticles properties will have a direct impact on the accuracy of calculated results. For this reason, in SUBTHAC code the thermophysical properties of nanoparticles are set as a function of temperature. The specific heats of nanoparticles are listed in Table 2 for some operational temperatures. To use these values in a numerical algorithm, polynomial interpolation can be expressed as:

$$Cp_{np} = a_1 T^3 + a_2 T^2 + a_3 T + a_4, \qquad (27)$$

where coefficient $a_{1\text{-}4}$ for each of the nanoparticles are listed in Table 4.

Table 4. The values of $a_{1\text{-}4}$ in equation (27)

Parameter	Al_2O_3	TiO_2	CuO
a_1	-3.947×10^{-9}	3.684×10^{-9}	2.539×10^{-9}
a_2	-4.785×10^{-6}	-3.638×10^{-6}	-2.218×10^{-6}
a_3	0.00235513	0.00150188	0.00084872
a_4	0.755614	0.656635	0.511279

3. Numerical Method

After preparation of subchannel equations and appending nanofluids correlations, the numerical method to solve the set of equations is to be chosen. FORTRAN programming language was adopted to develop SUBTHAC code. The flowchart of calculations is shown in Figure 4. At each axial level, coolant enthalpy, pressure and lateral mass flow rates are assumed first. By solving the subchannel equations, the initial values are modified. This step is applied for an axial node in all channels simultaneously. Finally, the numerical convergence is checked to determine whether another iteration is needed. Simple constant convergence criteria with a value of 0.001 were considered to get the convergence of parameters in each step. It took generally 20-30 iterations to achieve it for the parameters. The most important part of the

algorithm is the solution of the lateral momentum equation. To this end, the delta parameter, which represents the deviation of the assumptions from the real answers, is defined as follows:

$$\delta = \frac{\partial w}{\partial t} + \frac{\partial (wu)}{\partial z} - \frac{s}{l}[P_{l+\Delta l} - P_l] + \frac{1}{2}\frac{s}{l} k_G \frac{w|w|}{\rho^*_{nf} s^2}, \tag{28}$$

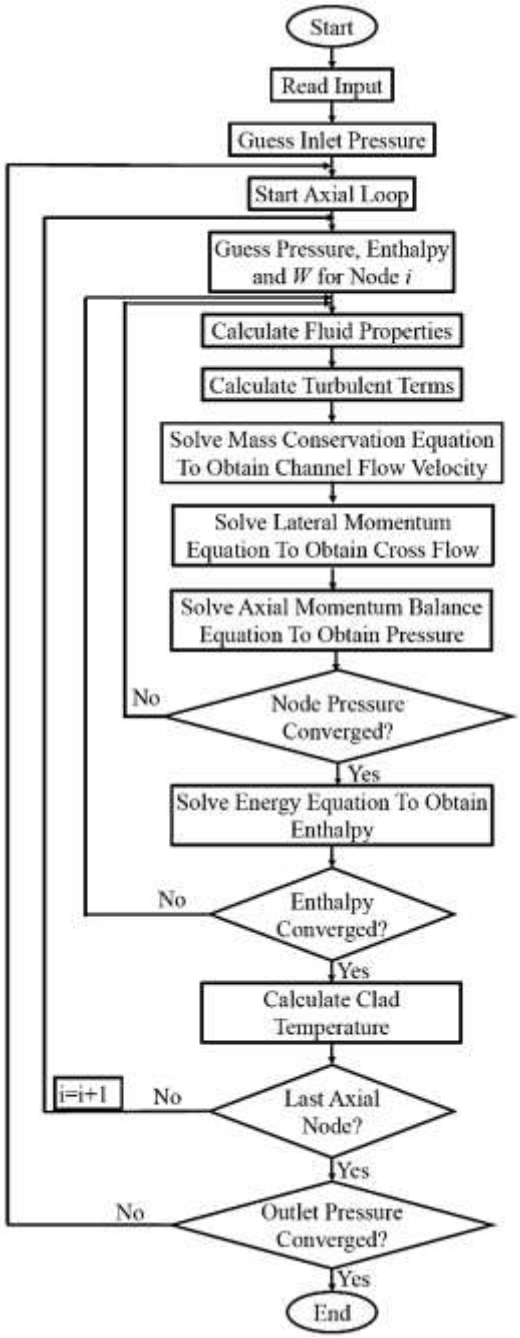

Figure 4. Flowchart of numerical calculations applied on subchannel approach in code SUBTHAC.

Therefore, the value of δ at iteration k is calculated as

$$\delta^k = \frac{\partial w^{k-1}}{\partial t} + \frac{\partial (w^{k-1}u^k)}{\partial z} - \frac{s}{l}\left[{P_{l+\Delta l}}^k - {P_l}^k\right] + \frac{1}{2}\frac{s}{l}k_G \frac{w^{k-1}|w^{k-1}|}{{\rho_{nf}^*}^k s^2}, \quad (29)$$

and the value of *w* is corrected as follows

$$w^k = w^{k-1} + F(\delta^k), \quad (30)$$

where *F* determines the degree of convergence to the real value.

4. On the Use of Boundary Conditions and Specific Heat of nanoparticles

As previously anticipated, two of the key choices to be made when nanofluids considered in NPPs are related to the (i) selection of the correct BCs for fluid flow (among inlet velocity/inlet mass flux/inlet Reynolds number) -that should be the same with base fluid to have meaningful comparison of results- and (ii) assumption of reliable values of thermo-physical properties of nanoparticles (such as, e.g., density and thermal conductivity) especially their specific heat at *reactor operational temperature*. The importance of these two choices can be better understood where the values of some thermal-hydraulic parameters for nanofluids (such as coolant outlet temperature and fuel clad temperature) are close to base fluid (water) and any error in these choices ((i) and (ii)) can strongly affect the results and, in some cases, damage the philosophy of using nanoparticles for thermal improvement of NPPs.

Different boundary conditions such as pressure, temperature, velocity and mass flux can be selected to solve the set of subchannel equations. The main challenge that has been raised is the selection (equal to base fluid) of one of the following conditions: (i) inlet velocity, (ii) inlet mass flux, (iii) inlet Reynolds number. Selecting each of these BCs (in addition to others BCs like inlet temperature and outlet pressure) along with values of specific heat for nanoparticles can affect the thermal-hydraulic results of nanofluids.

Specific heat capacity is one of the thermo-physical parameters that in addition to it is explicit effect on energy conservation equation (equation 11), it is used as one of the main factors in calculating the *Nu* number and $h_{convection.}$. Table 2 lists the specific heat of the three so far most studied nanoparticles [25]. As it is evident, values of specific heats are changing of a percentage of 20-40% between 25 ºC (standard state) and 320 ºC (NPPs operational temperature), a circumstance that proves the importance of selecting the correct values for these parameters.

In some notably studies ([8,10,12,30–34] among others), due to lack of data, the values of specific heat capacity of nanoparticles at 25 ºC were incorrectly adopted and used for

calculations in NPPs under *operational temperatures (around 300 ^{o}C)*. This incorrect input parameter along with applied BCs (inlet mass flux instead of inlet velocity that is a design parameter) have affected the results achieved in those articles, damaged their conclusions about using nanofluids and wrongly proposed some incorrect modifications. In some of these cases, despite enhancing the heat transfer coefficient in the presence of nanoparticles, safety parameters (clad temperature margin) weren't improved as excessive increase in fluid temperature, that is a direct result of the wrong specific heat capacity value. For an additional explanation, it should be noted that the stated main goals of using nanoparticles in these publications were:

a) to increase the outlet temperature of the core (by enhancing heat transfer in the reactor core) and improve the plant efficiency;
b) to improve the convective heat transfer coefficient, lead to a reduction of clad temperature and an increase of safety margin for fuel.

However, it should be remarked that changes in the specific heat capacity have opposite effects with respect to goals a) and b). In particular, on the one hand, by increasing the specific heat of fluid, the outlet temperature reduces whereas, on the other, the ability of heat removal from fuel structure increases (clad and fuel temperature decrease). These conflicting effects import some complexities and errors in the results if the correct BCs and value of specific heat in the relevant temperature are not used in the analysis. Effects of selecting different BCs and right assumptions of specific heat of nanoparticles will be shown and discussed in detail in the next section.

5. Results and Discussion

The new computer code 'SUBTHAC' was developed as described based on the subchannel approach and the nanofluid module was added to its kernel give the ability of thermal-hydraulic analysis of reactor core by nanofluid coolants. Validation of the code output was conducted in two steps. In the first one, the thermal-hydraulic results of water as coolant are compared to the values obtained by COBRA-EN code [35] (COBRA-EN has been executed in three equations mode). In the second step, the results of SUBTHAC nanofluid analysis are validated with the results of a CFD analysis reported in reference [36]. Finally, the nanofluid module was used to calculate the thermal-hydraulic parameters with nanofluids as coolant. The comparison between the results of these three steps reveal the effects of nanoparticles on thermal-hydraulic parameters.

For the first step, the rectangular rod bundle is considered as a case study. The geometry is shown in Figure 5. The selected case study is one of the worst-case from the point of the complexity of the calculations for subchannel approach as there are 3 different channels connected and their hydraulic diameters are different (unlike reactor core that hydraulic diameters are the same and help to the simplicity of calculations). The problem is comprised of four fuel rods, three types of channels (total 9 channels) and two types of gaps (total 12 gaps) that have been mentioned in Figure 5. Convective equations were solved in the hottest channel to compare the clad outside temperature which is shown by point 1. Note that the heat fluxes of all fuel rods are equal and uniform for all nodes in the axial direction. The boundary conditions that are considered for both water and nanofluids are listed in Table 5.

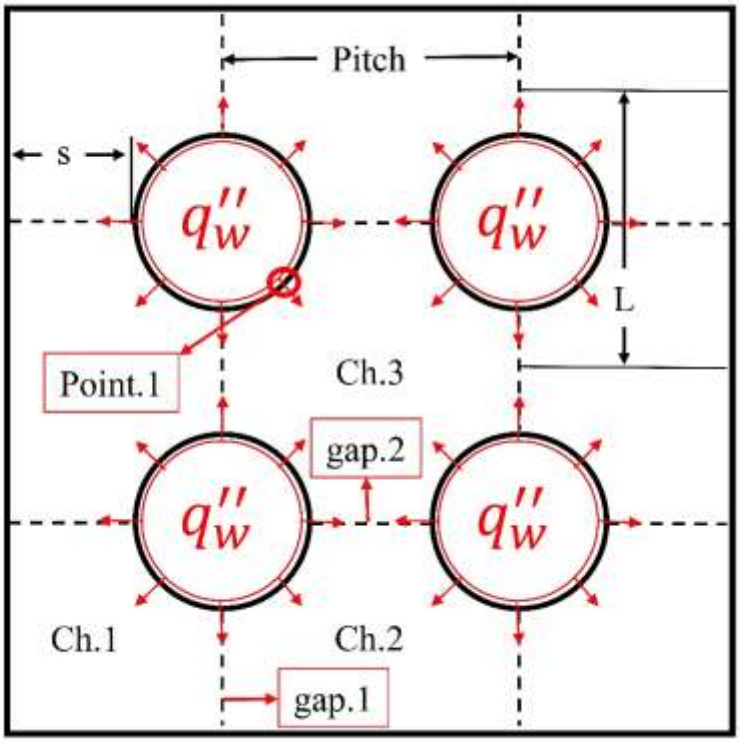

Figure 5. Geometry and subchannel layouts of the 4-rod bundle case study.

Table 5. Boundary conditions for 4-rods assembly

Pitch [mm]	Rod to wall distance (s) [mm]	Rod diameter [mm]	Height [m]	q''_{ave} [kW/m^2]	u_{inlet} [m/s]	P_{outlet} [MPa]	T_{inlet} [°C]
13.2	3.6 mm	10 mm	3.5	653.13	4.243	15.8	291.3

Figures 6 to 8 gather data for the validation of the results provided by SUBTHAC against those of the COBRA-EN code. These figures show the axial channel temperature, mass flux of three

channels and the mass flow per unit length in the lateral direction (W) for two gaps. It is first noted that the temperature increases almost linearly with the axial height. As expected, among the three, channel 3 has the highest temperature as it receives more heat flux by the four fuel rods (Figure 6).

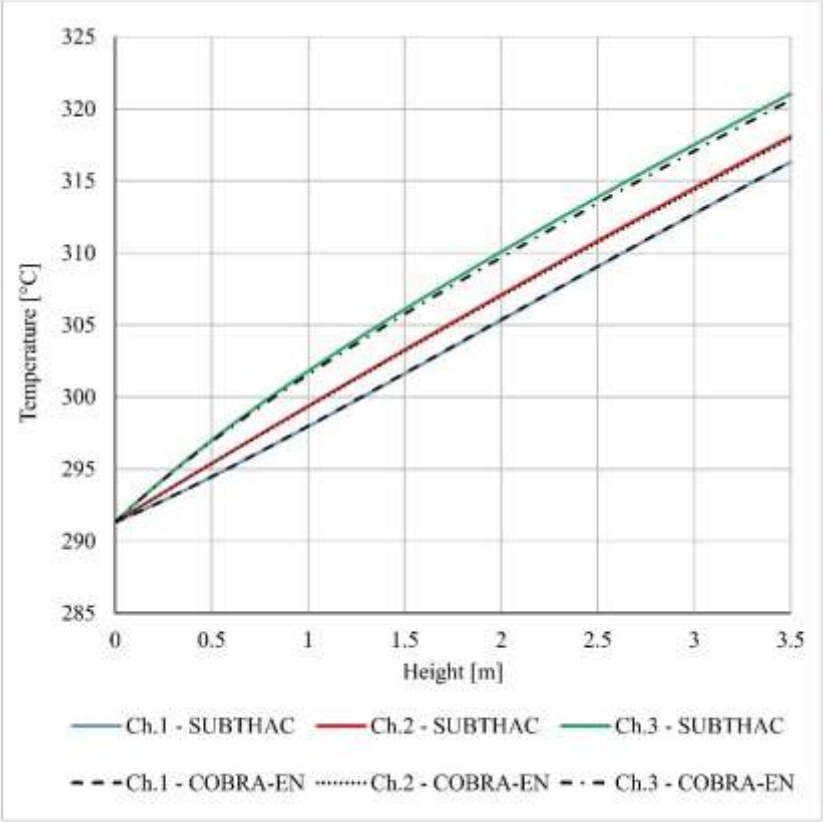

Figure 6. Benchmarking of temperature profiles of three subchannels calculated by SUBTHAC code against those obtained by COBRA-EN.

As channel 3 has the largest hydraulic diameter (i.e. shortest wetted perimeter) in comparison with channel 1 and 2, its mass flux increases along upward flow (Figure 7). Channel 2 has almost equal incoming and outgoing masses from and to its adjacent channels, so its mass flux will be almost constant. Since no mass accumulation is present in this geometry, the amount of mass flux for channel 1 should decrease. Figure 8 presents the profile of mass flux in lateral directions among gaps. Values of lateral mass flux decreases with channel height. This is due to the fact that, by increasing the height, subchannels tend to have equal pressures so that the lateral flow is reduced.

Results of Figures 6 to 8 are in good agreement with the output computed by COBRA-EN; this proves the validity of SUBTHAC that can then be employed for nanofluid calculations. Further assessment of the validity of the new code has been conducted by inspecting outlet fluid

temperature and mass flux of each subchannel, as reported in Table 6. The proximity of values of outlet temperature and mass flux of each subchannel with those provided by COBRA-EN is another evidence of the reliability of SUBTHAC code.

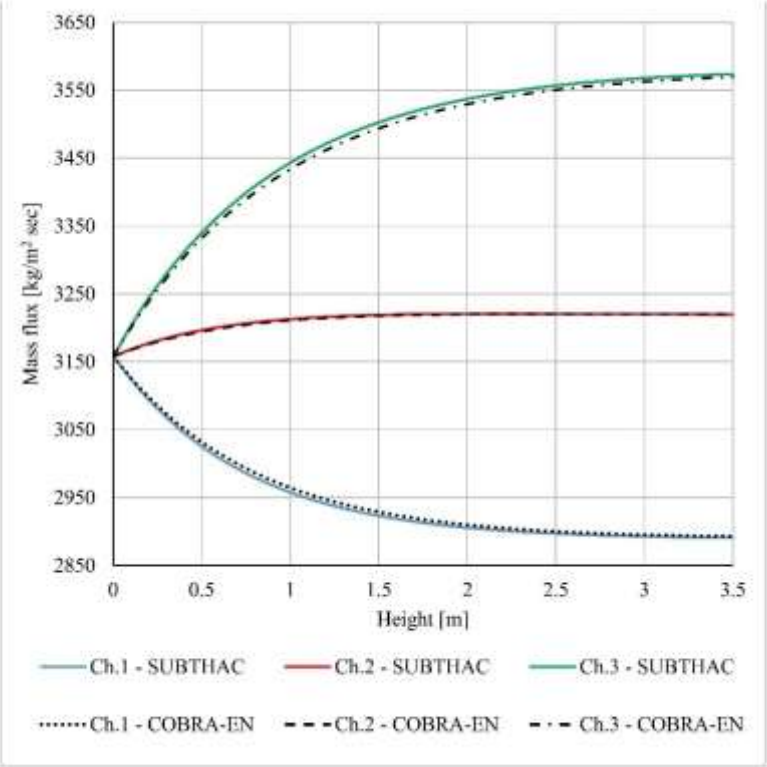

Figure 7. Benchmarking of mass flux profiles calculated by SUBTHAC code against those obtained by COBRA-EN.

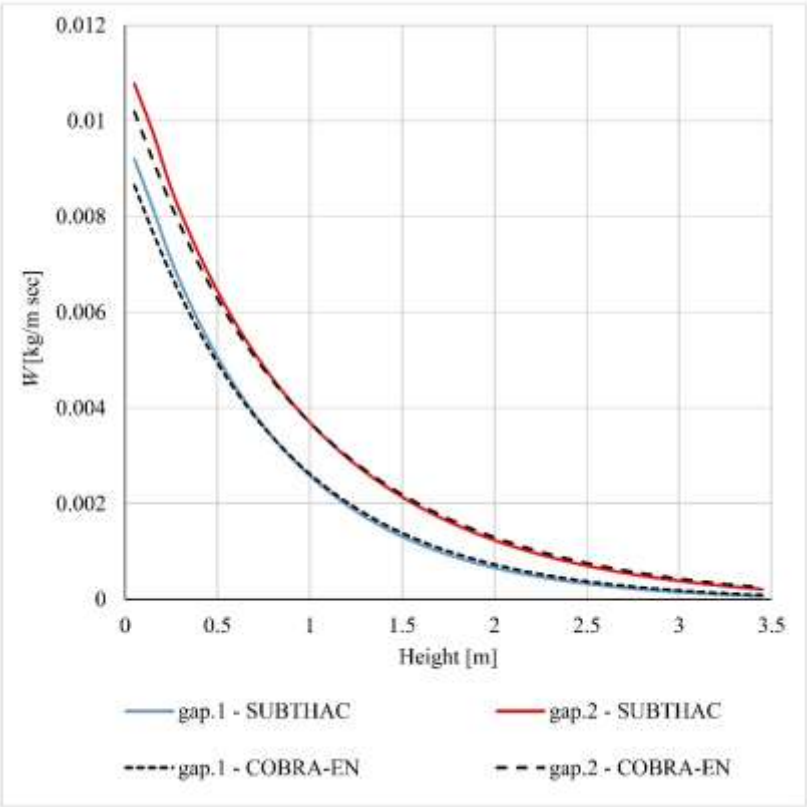

Figure 8. Benchmarking of profiles of lateral mass flow through gaps calculated by SUBTHAC code against those obtained by COBRA-EN.

Table 6. Comparisons of outlet fluid temperature and mass flux

Thermal-hydraulic code		T [°C]	Mass Flux [kg/m^{2}s]
SUBTHAC	Ch.1	316.31	2890.6372
	Ch.2	318.09	3219.6401
	Ch.3	321.04	3573.7866
	Average	317.92	3158
COBRA-EN	Ch.1	316.33	2892.6840
	Ch.2	317.94	3219.5554
	Ch.3	320.62	3569.4021
	Average	317.79	3158

In the second step, to validate the performance of the SUBTHAC code in nanofluid analysis, the results of the code are compared with the results of obtained carrying out CFD simulations [36]. The studied geometry is a single square channel (Figure 9) that has been analyzed for pure water and 3% volume concentration of water/alumina (Al_2O_3) nanofluid. The applied boundary conditions are tabulated in Table 7. Other assumptions such as thermophysical properties and physical characteristics of the case study can be found in [36].

Table 7. Boundary conditions for the single square channel case [36]

Pitch [mm]	Rod diameter [mm]	Height [m]	q''_{ave} [kW/m^2]	u_{inlet} [m/s]		P_{outlet} [MPa]	T_{inlet} [K]
				Pure water	3% Al_2O_3		
11.875	9.5	0.6	600 uniform	7.829	9.196	15.51	569

Figures 10 and 11 show averaged temperature and pressure profiles at different channel heights. The data show good agreement between the results of SUBTHAC code with those calculated via CFD simulations [36] for both pure water and nanofluids. The small discrepancies relate to the different numerical methods of analysis, convergence criteria, thermophysical properties functions of SUBTHAC and CFD software, etc. The comparison can prove the reliability of SUBTHAC code for both base fluid (pure water) and nanofluids analyses for different problems and geometries.

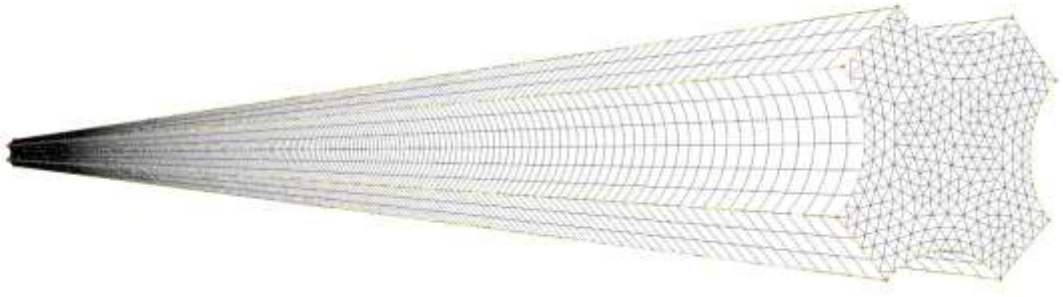

Figure 9. Single square channel geometry and its meshing for CFD simulations [36]

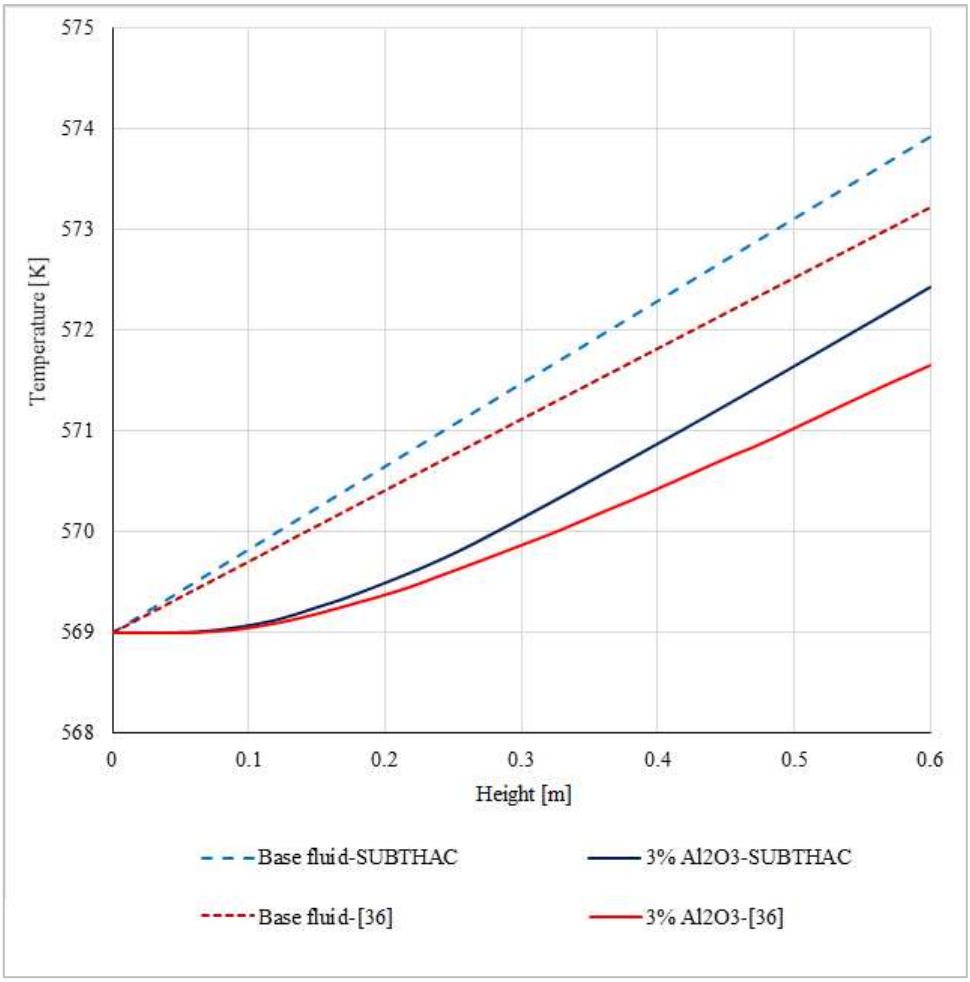

Figure 10. Temperature profile of SUBTHAC code and CFD simulations [36]

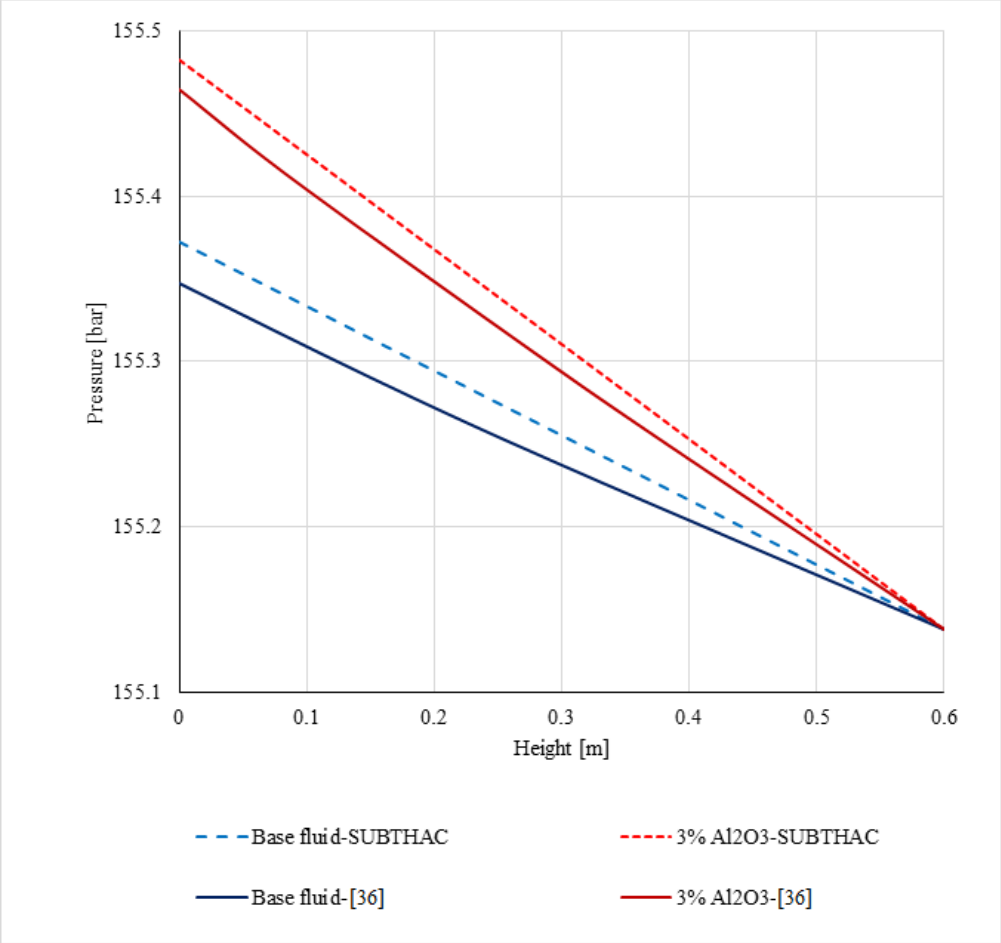

Figure 11. Pressure profile of SUBTHAC code and CFD simulations [36]

After validation of SUBTHAC code, the nanofluid module of SUBTHAC is used to analyze the effect of nanofluids on heat transfer and thermal-hydraulic parameters. To achieve this goal, the same 4-rod geometry of the first step is solved by adding the concerned nanoparticle to the base fluid. Average fluid temperature (averaged over subchannels along with flow) and clad temperature are used as reference indications to analyze the effect of nanofluids on the thermal-hydraulic parameters of coolant. For this purpose, Figure 12 shows average fluid temperature and clad temperature for water as base fluid coolant that were calculated in the first step.

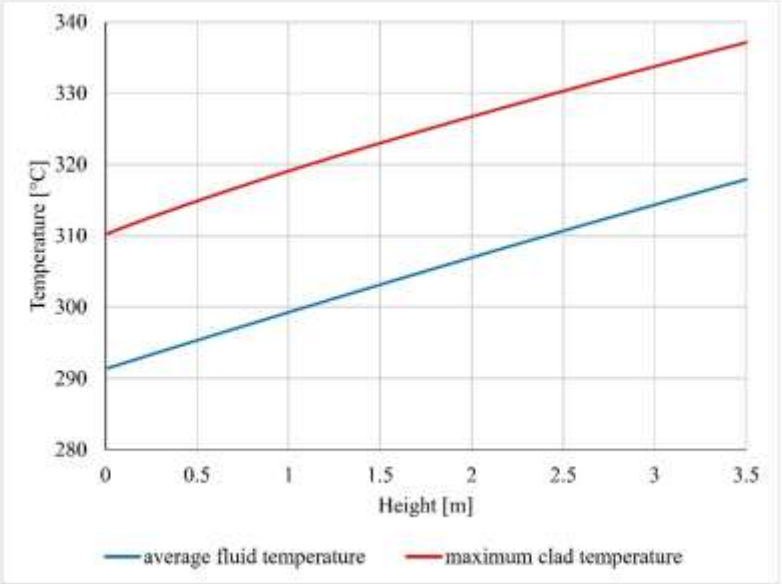

Figure 12. Average fluid and maximum clad temperatures for base fluid calculated by SUBTHAC code.

Nanofluid averaged-flow temperature deviations from that of base fluid (water) are shown in Figure 13 for 1%, 3% and 5% concentration of Al_2O_3, TiO_2 and CuO nanoparticles. It can be noted that the average fluid temperature for TiO_2 and CuO nanofluids are ascending function of both nanoparticle concentration and channel height meaning that by increasing the concentration of TiO_2 and CuO nanofluids the temperature of fluid will increase. This proves the efficiency of nanofluids in comparison with water, a result that benefit the overall reactor efficiency. An interesting point is that unlike other nanofluids, the temperature of the Al_2O_3 one starts with a negative deviation from base water. This means that nanofluid average temperature decreases up to the initial 2.5 m of channel height in comparison to that of base fluid. This descending function is proportional to the nanoparticle concentration. Beyond the height 2.5 m, the behaviour of Al_2O_3 nanofluid changes and behaves as that of nanofluids with TiO_2 and CuO nanoparticles. In analogy to the base water case (Table 6), the deviation of the outlet nanofluid temperature from base water are listed in Table 8 for each subchannel. The data lead to the following remarks: i) the most positive deviation from base water occurs in channel 3 outlet for all concentration of all nanofluids (channel 3 has the most heat flux) as the energy transfer between channels as result of turbulence, i.e. term $W'\Delta h$, is reduced in comparison with base water.

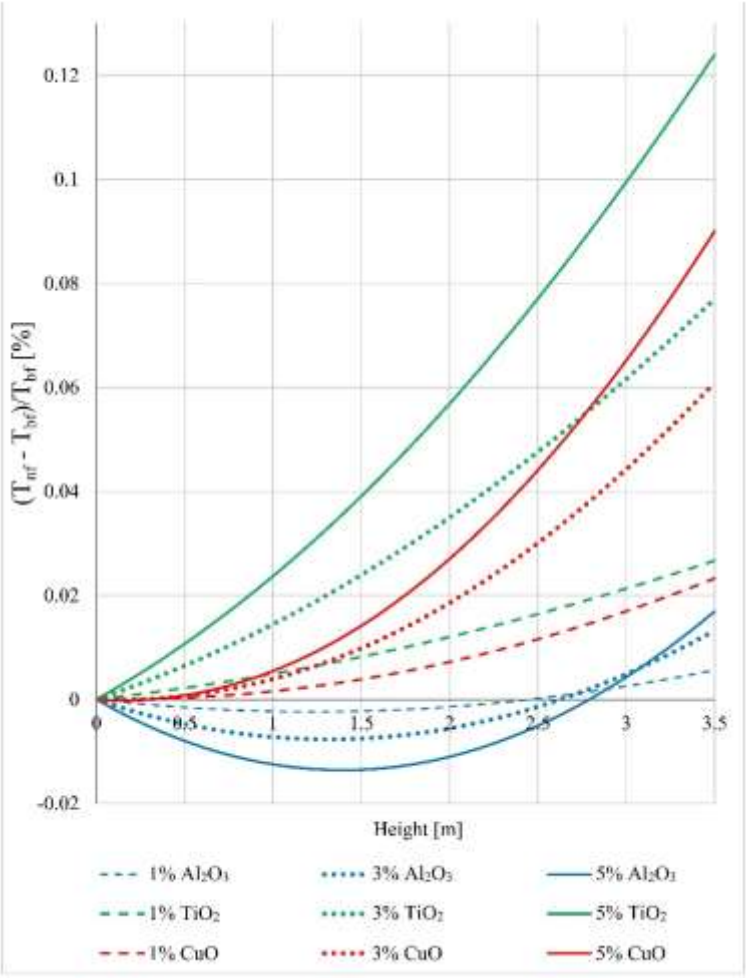

Figure 13. Percentage deviation from base fluid of averaged flow temperature computed for the three different nanofluids with three different concentrations.

It should be noted that in this term, W' increases, but as Δh decreases with more power, this term reduces overall. These results are shown in Figure 14 by comparing the values of $W'\Delta h$. ii) nanofluids based on CuO and Al_2O_3 particles have negative deviation for their all concentrations in channel 1 outlet, while these amount become positive for average channel outlet (see red and blue curves in Figure 13) as their positive deviations in subchannel 2 and 3 can change the average of these values to a positive one (it is important to note that this procedure hasn't take place for Al_2O_3 in the initial 70% of channel height as evident in Figure 13).

Table 8. Deviation of outlet nanofluids temperatures from base fluid (pure water).

Nanoparticle	Deviation percentage $(T_{nf} - T_{bf})/T_{bf}$ [%]		
	Ch.1	Ch.2	Ch.3
Al_2O_3 1%	- 0.00552	0.006571	0.027651
Al_2O_3 3%	- 0.01697	0.015748	0.073113
Al_2O_3 5%	- 0.02855	0.020574	0.107175
TiO_2 1%	0.011756	0.028002	0.055909
TiO_2 3%	0.035098	0.080664	0.159301
TiO_2 5%	0.058685	0.129659	0.252671
CuO 1%	- 0.00464	0.025758	0.078016
CuO 3%	- 0.01479	0.067475	0.21007
CuO 5%	- 0.0241	0.099647	0.315671

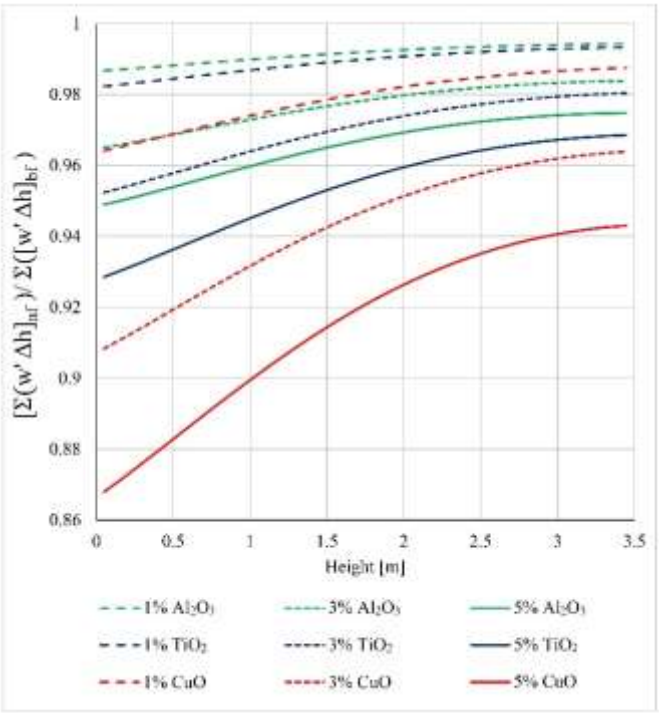

Figure 14. Deviations of the term $W'\Delta h$ (lateral energy transfer by turbulent mixing) of nanofluids from that of the base fluid.

The averaged percent deviation of quantities w (i.e. mass flow per unit length in the lateral direction through the gap) and w' (i.e. turbulent mixing flow rate per unit length through the gap) are presented in Table 9. While Al_2O_3 and TiO_2 nanofluids have almost the same positive deviation against base fluid, the maximum amount of deviation can be seen for CuO. The values of the outlet to inlet mass flux were also listed in Table 10. According to this table, values of outlet to inlet mass flux are lower than unit for subchannel 1 and more than unit for

subchannels 2 and 3. These were expected analogy to base fluid (Figure 7) and the same reasons.

Table 9. Average deviation of w and w' from base fluid.

Nanoparticle	$(w_{nf} - w_{bf})/ w_{bf}$ [%]		$(w'_{nf} - w'_{bf})/w'_{bf}$ [%]	
	gap. 1	gap. 2	gap. 1	gap. 2
Al_2O_3 1%	4.604	4.649	4.151	4.163
Al_2O_3 3%	13.810	13.955	12.485	12.526
Al_2O_3 5%	23.036	23.296	20.868	20.941
TiO_2 1%	4.480	4.513	4.065	4.075
TiO_2 3%	13.440	13.548	12.229	12.260
TiO_2 5%	22.425	22.623	20.440	20.498
CuO 1%	7.963	7.991	7.079	7.084
CuO 3%	23.911	24.011	21.224	21.240

Table 10. Outlet to inlet mass flux for base fluid and nanofluids.

	Ch.1	Ch.2	Ch.3
Base fluid	0.915338	1.019519	1.131661
Al_2O_3 1%	0.915126	1.019549	1.132049
Al_2O_3 3%	0.914739	1.019602	1.132762
Al_2O_3 5%	0.914393	1.019646	1.133412
TiO_2 1%	0.91515	1.019549	1.131995
TiO_2 3%	0.914803	1.019601	1.132619
TiO_2 5%	0.914488	1.019645	1.133199
CuO 1%	0.915058	1.019572	1.132131
CuO 3%	0.914575	1.01966	1.132955
CuO 5%	0.91417	1.019728	1.133665

Figure 15 shows the deviation of clad outside temperature in the case of nanofluid from base fluid. As this figure shows, clad outside temperatures have been decreased in the case of using nanofluid in comparison with using base fluid and it can be one of the main goals and advantages of using nanofluids in nuclear power plants. Reductions in clad temperature using nanofluids is proportional to nanofluids concentrations, as more concentration leads to more clad temperature decrease. The main reasons for this issue are changes in fluid temperature and heat convection coefficient.

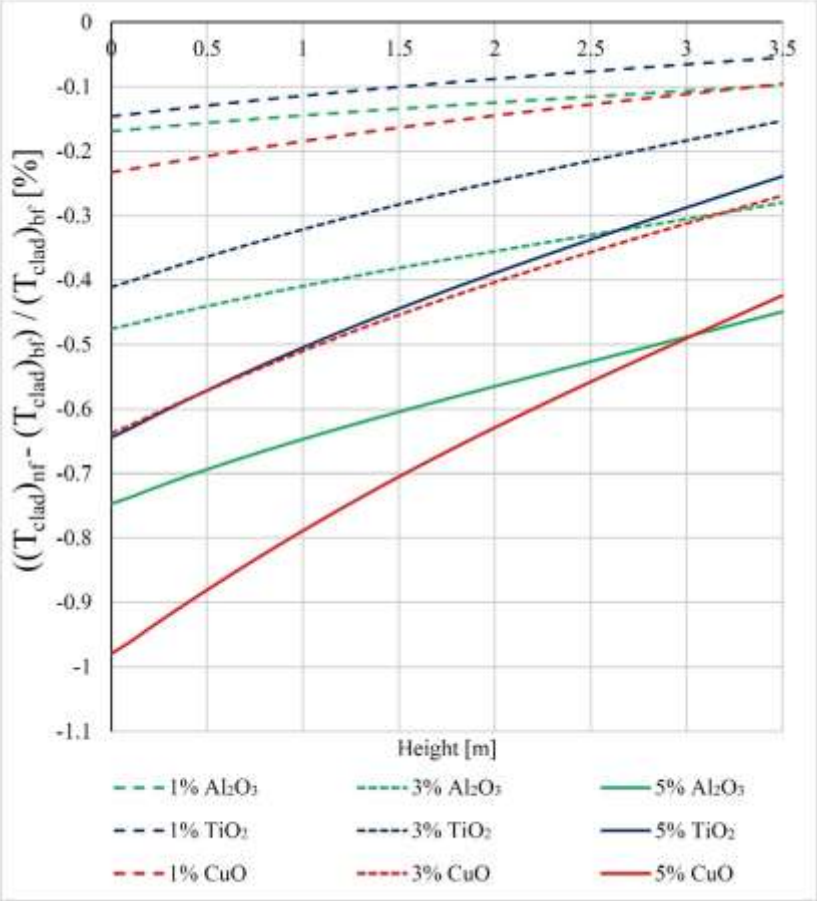

Figure 15. Deviations of clad outside temperature computed for nanofluids from that when only base fluid in employed.

Figure 16 shows the profile of deviation of heat convection coefficient for nanofluids from the base fluid. This figure can confirm that using nanofluid increase the heat convective coefficient and by this mean lead to reduce the clad outside temperature (more heat removal) and improve the safety margins.

One of the most important challenges in the use of nanofluids instead of base fluid (water) is the pressure drop issue. Nanoparticles can increase the amount of pressure drop in the reactor core and cause some of the defects like fouling or plate out. Figure 17 shows the deviation of pressure drop in the presence of nanofluid from base fluid. As can be understood from this figure, by increasing the concentration of nanofluids (regardless of its type), the pressure drop will increase. It does not seem that increasing the pressure drop more than 15-20 % can be justifiable from nuclear economy and plant cost points. Values of total pressure drop for nanofluids and base fluid are also listed in Table 11.

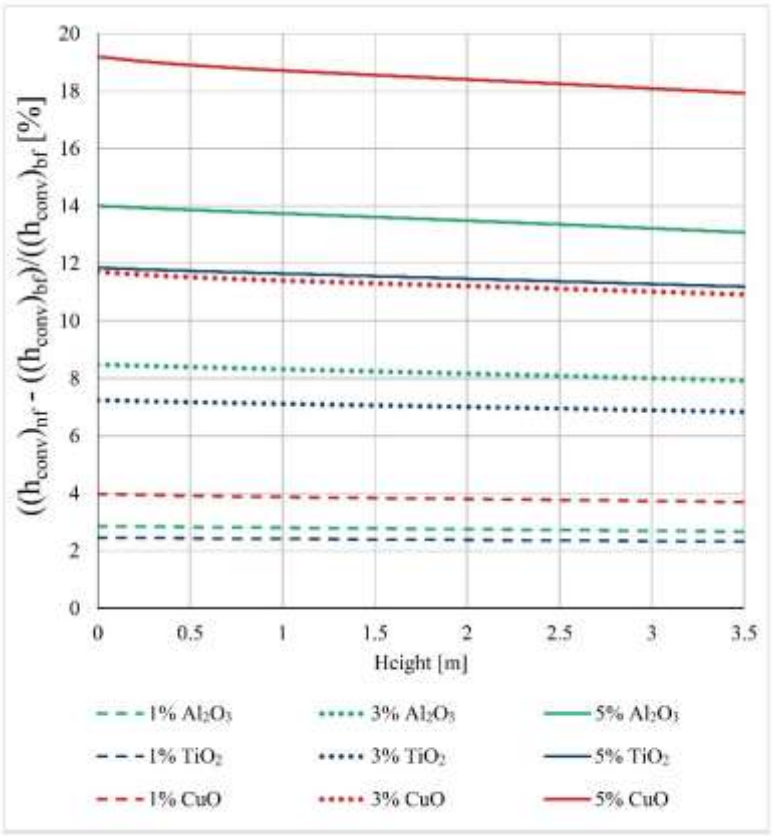

Figure 16. Deviations of convective heat transfer coefficient computed for nanofluids from that when only base fluid in employed.

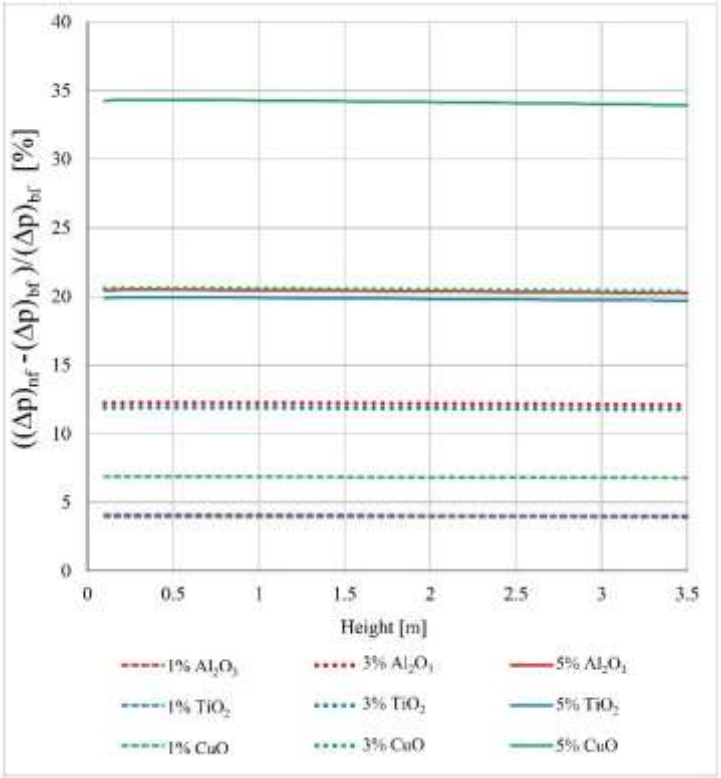

Figure 17. Deviations of pressure drop computed for nanofluids from that when only base fluid in employed.

Table 11. Comparison between nanofluid and base fluid pressure drops [kPa].

Nanoparticle	Concentration of nanoparticle		
	1 %	3 %	5 %
ΔP_{Al2O3}	62.98	67.84	72.73
ΔP_{TiO2}	62.94	67.70	72.50
ΔP_{CuO}	64.68	72.90	81.13
Base fluid (Pure water)	60.57		

In the final discussion of this section, the effects of BCs (equal inlet velocity/inlet mass flux/inlet Reynolds number with base fluid, that means that values of these parameters are chosen as the same as those employed for base fluid calculations) and correct values of specific heat of nanoparticles (constant value or temperature depended one) are presented in Figures 18 to 20. Figures 18 and 19 show average channel temperature profiles and their deviation from base fluid for TiO_2, respectively. As it can be seen in Figure 18, the predicted values of temperature profiles are different for various BCs and specific heats. Results of *constant specific heat and equal inlet Reynolds number method* are closer to this study (*Temperature dependent specific heat and equal inlet velocity method*) in comparison to those obtained for *equal inlet mass flux*.

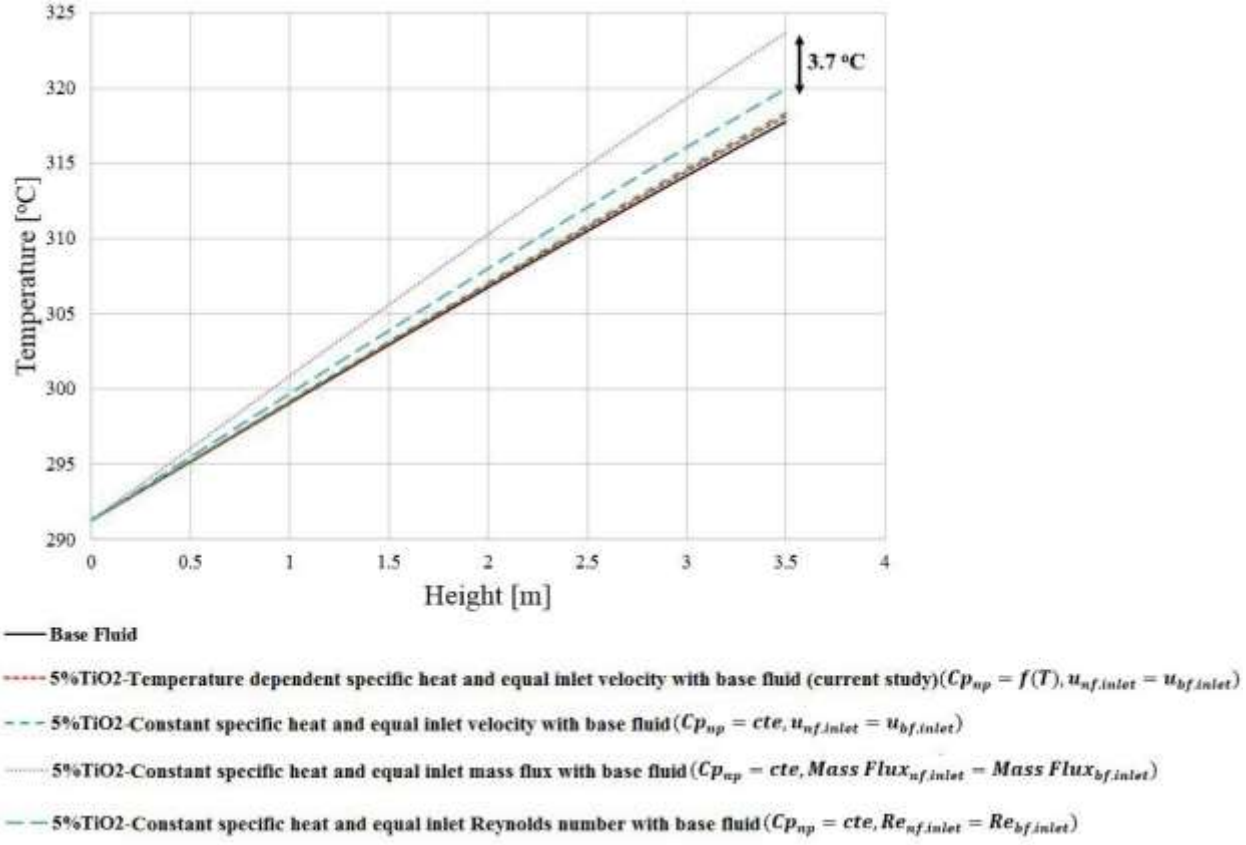

Figure 18. Nanofluids' average channel temperature profiles for different applied BCs and specific heat

These differences are more obvious in Figure 19, as results of *constant specific heat and equal inlet mass flux method* (that have been applied to the articles cited in section 4) are very far from other types of calculations.

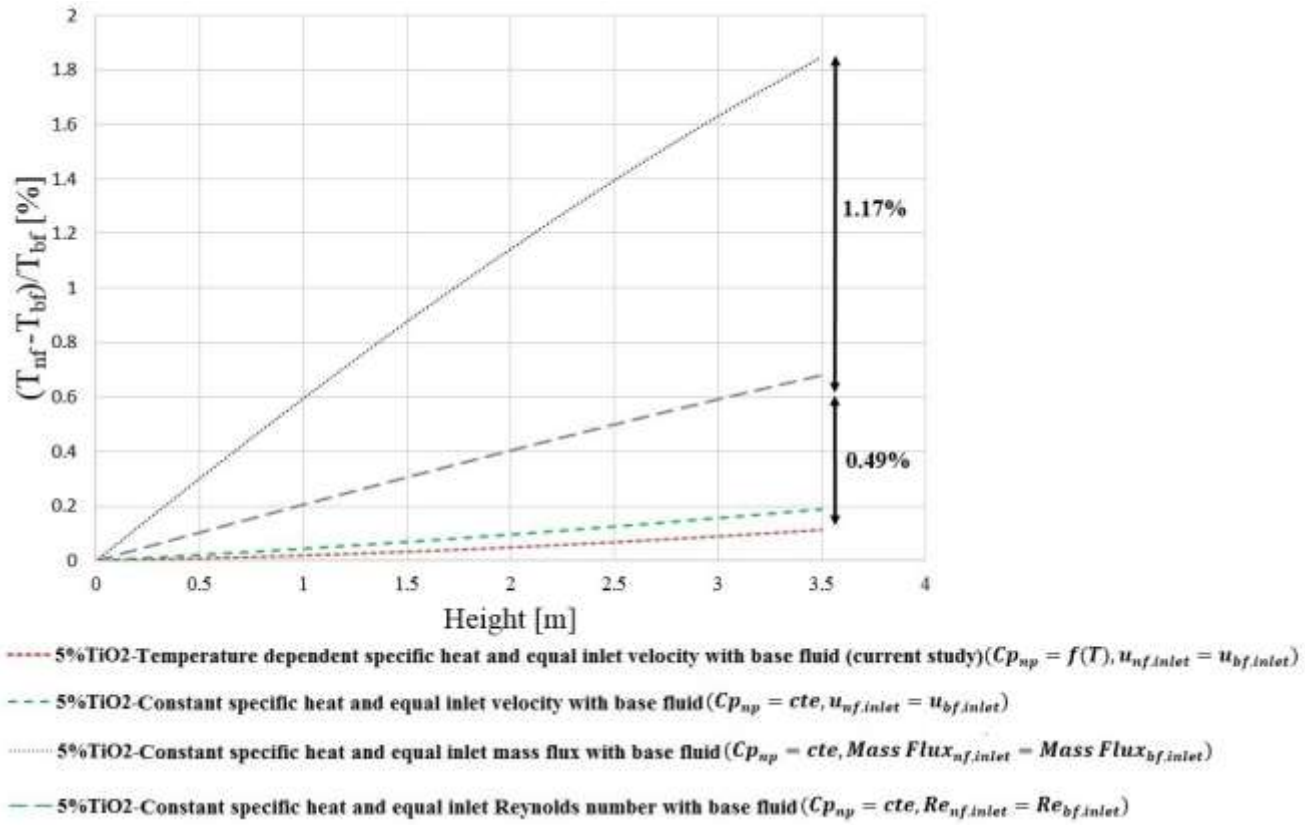

Figure 19. Deviations of nanofluids' average channel temperature from base fluid for different applied BCs and specific heat

These dissimilarities are more interesting and complex in the case of the outside temperature of clad, as shown in Figure 20. Unlike the other methods, values of clad outside temperature has risen up by using *constant specific heat and equal inlet mass flux method* even in comparisons to base fluid. This method has been applied on cited articles in section 4 and it can make this question that what is the point of using nanofluid that while they are increasing outlet temperature (lead to better efficiency), also increasing the clad outside temperature (disadvantages and risk of safety issue). It should be considered that if the goal of using nanofluid is to increase the outlet temperature without modifying the safety margins, it can be done only with increasing NPPs power without the need to using nanofluids! Unfortunately, this wrong conclusion has been stated in some previous articles (mentioned in section 4) because of the wrong values for specific heat and equal inlet mass flux as BC.

Using *temperature-dependent specific heat and equal inlet velocity method* and *constant specific heat and equal inlet Reynolds number method* have more better result as by applying both of these methods, clad temperature has also decreased in the presence of nanofluids (Figure 20) and profiles of these two methods are closer and reliable.

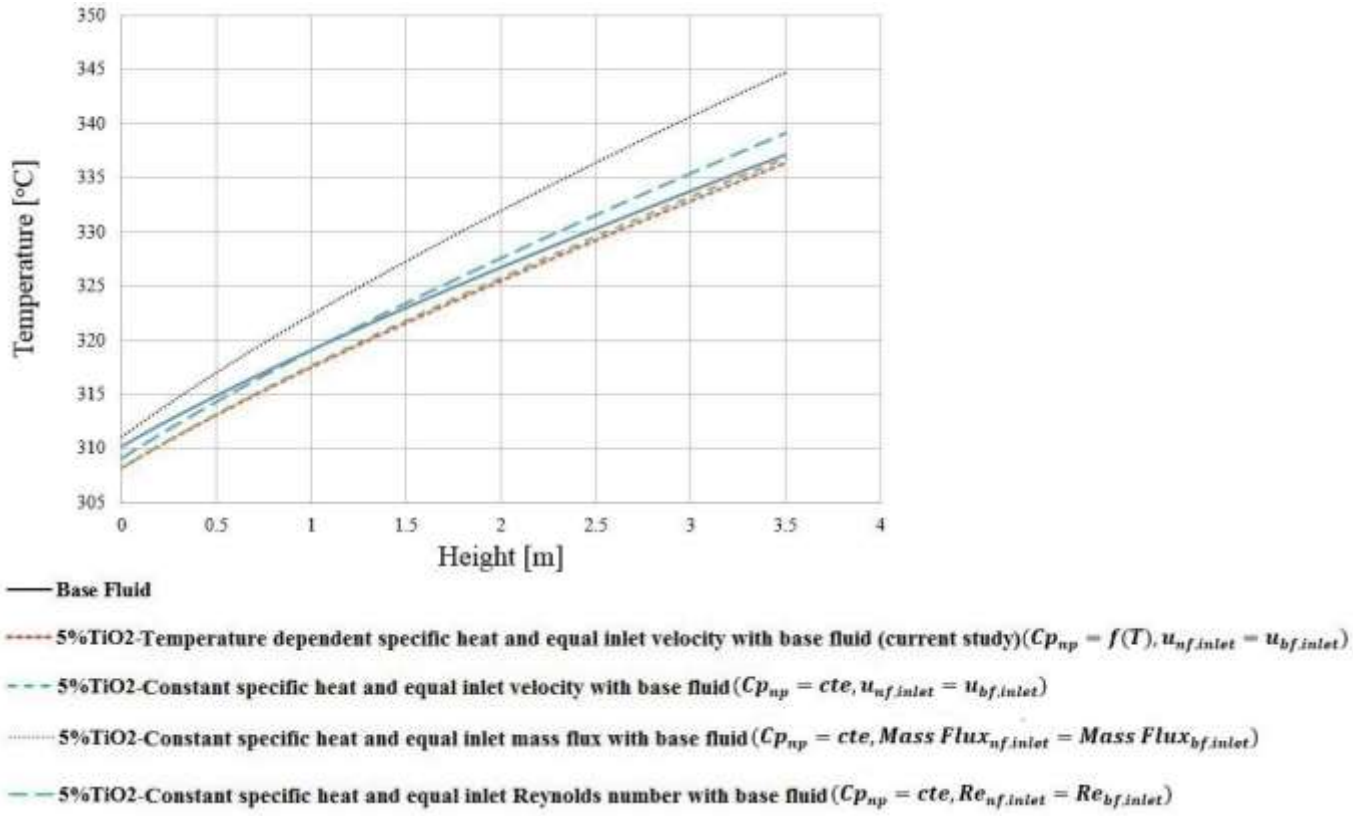

Figure 20. Nanofluids' clad outside temperature profiles for different applied BCs and specific heat.

6. Conclusions

Nanofluids are currently investigated by the research community as they are promising candidates to be used in the future of NPPs to improve efficiency and safety. In this article, a new code is developed for thermal-hydraulic analysis of nanofluids employed in the reactor core. This new code, called 'SUBTHAC', uses the subchannel approach to estimate the effects of adding nanoparticles to the base fluid on thermal-hydraulic parameters of the reactor. The main outcomes of the article can be summarized as follows:

- A key aspect of applying subchannel approach is to include the lateral turbulence parameter in the energy equation to explore the possibility of using nanofluid as a coolant.

- Analyzing the nanofluid application in NPPs should be considered as a multi-objective analysis, as in some cases by improving one of the parameters (e.g. outlet flow temperature), safety margin of other parameters (e.g. clad temperature) may be reduced.
- The addition of Al_2O_3, TiO_2 and CuO nanoparticles is justifiable up to a concentration of 3% volume of base fluid; beyond this threshold, a large pressure drop in the reactor core is induced, a condition that is not acceptable from both thermal-hydraulic design and economic points of view.
- The selection of the nanofluid among the three that have been investigated is strongly dependent on the final goal. If this coincides with reaching a higher fluid outlet temperature, TiO_2 is the optimal choice (CuO and Al_2O_3 follow in this order), whereas when the goal is to decrease the fuel structure temperature (clad and fuel), CuO is the best selection, followed, in order, by Al_2O_3 and TiO_2.
- One of the key messages of the paper is to assume the thermo-physical properties of nanoparticles as a function of temperature, so that their correct values at the *operational temperature of NPPs* are correctly captured by the numerical tool. This assumption revealed to be crucial in order to predict correctly the coolant and fuel temperatures.
- In addition to the previous point, selecting one of the inlet boundaries conditions among inlet velocity/inlet mass flux/inlet Reynolds number can affect remarkably the results.
- It is NOT recommended the simultaneous use of *inlet mass flux boundary condition* and *constant specific heat capacity* within subchannel approach as this combination method can affect the validity of nanofluids' results and even, in some cases, generate wrong or antithetical outcome.
- As the inlet velocity of coolant is one of the main design parameters of NPPs, reported in any FSAR, it can be selected as the most reliable boundary condition in the numerical calculations.

Although using nanofluids as new coolant in NPPs can modify some thermal-hydraulic parameters of reactor core, more theoretical and experimental research is needed to assess practical implementation. Applying different models and simulations methods such as the two-phase model (considering nanoparticles as individual phase) can lead to more reliable results.

Acknowledgment

Part of this research has been developed under the auspices of European Union Horizon 2020 research and innovation programme Marie Skłodowska-Curie Actions COFUND grant SIRCIW, agreement no. 663830.

7. References

[1] J. Buongiorno, L.-W. Hu, S.J. Kim, R. Hannink, B. Truong, E. Forrest, Nanofluids for Enhanced Economics and Safety of Nuclear Reactors: An Evaluation of the Potential Features, Issues, and Research Gaps, Nucl. Technol. 162 (2008) 80–91. doi:10.13182/NT08-A3934.

[2] J. Buongiorno, L. Hu, Nanofluid Heat Transfer Enhancement for Nuclear Reactor Applications, in: ASME 2009 Second Int. Conf. Micro/Nanoscale Heat Mass Transf. Vol. 3, ASME, 2009: pp. 517–522. doi:10.1115/MNHMT2009-18062.

[3] J. Buongiorno, Convective Transport in Nanofluids, J. Heat Transfer. 128 (2006) 240. doi:10.1115/1.2150834.

[4] H.Ş. Aybar, M. Sharifpur, M.R. Azizian, M. Mehrabi, J.P. Meyer, A Review of Thermal Conductivity Models for Nanofluids, Heat Transf. Eng. 36 (2015) 1085–1110. doi:10.1080/01457632.2015.987586.

[5] J.P. Meyer, S.A. Adio, M. Sharifpur, P.N. Nwosu, The Viscosity of Nanofluids: A Review of the Theoretical, Empirical, and Numerical Models, Heat Transf. Eng. 37 (2016) 387–421. doi:10.1080/01457632.2015.1057447.

[6] R.B. Ganvir, P.V. Walke, V.M. Kriplani, Heat transfer characteristics in nanofluid—A review, Renew. Sustain. Energy Rev. 75 (2017) 451–460. doi:10.1016/J.RSER.2016.11.010.

[7] S.K. Das, S.U.S. Choi, H.E. Patel, Heat Transfer in Nanofluids—A Review, Heat Transf. Eng. 27 (2006) 3–19. doi:10.1080/01457630600904593.

[8] K. Hadad, A. Rahimian, M.R. Nematollahi, Numerical study of single and two-phase models of water/Al2O3 nanofluid turbulent forced convection flow in VVER-1000 nuclear reactor, Ann. Nucl. Energy. 60 (2013) 287–294. doi:10.1016/j.anucene.2013.05.017.

[9] K. Hadad, Z. Kowsar, Twofold application of nanofluids as the primary coolant and reactivity controller in a PWR reactor: Case study VVER-1000 in normal operation, Ann. Nucl. Energy. 97 (2016) 179–182. doi:10.1016/J.ANUCENE.2016.07.008.

[10] E. Zarifi, G. Jahanfarnia, F. Veysi, Thermal–hydraulic modeling of nanofluids as the coolant in VVER-1000 reactor core by the porous media approach, Ann. Nucl. Energy. 51 (2013) 203–212. doi:10.1016/j.anucene.2012.07.041.

[11] S.M. Mousavizadeh, G.R. Ansarifar, M. Talebi, Assessment of the TiO2/water nanofluid effects on heat transfer characteristics in VVER-1000 nuclear reactor using CFD modeling,

Nucl. Eng. Technol. 47 (2015) 814–826. doi:10.1016/j.net.2015.07.001.

[12] V. Ghazanfari, M. Talebi, J. Khorsandi, R. Abdolahi, Thermal–hydraulic modeling of water/Al2O3 nanofluid as the coolant in annular fuels for a typical VVER-1000 core, Prog. Nucl. Energy. 87 (2016) 67–73. doi:10.1016/J.PNUCENE.2015.11.008.

[13] O. Safarzadeh, A.S. Shirani, A. Minuchehr, F. Saadatian-derakhshandeh, Coupled neutronic/thermo-hydraulic analysis of water/Al2O3 nanofluids in a VVER-1000 reactor, Ann. Nucl. Energy. 65 (2014) 72–77. doi:10.1016/J.ANUCENE.2013.10.036.

[14] D. Sharma, K.M. Pandey, A. Debbarma, G. Choubey, Numerical Investigation of heat transfer enhancement of SiO2-water based nanofluids in Light water nuclear reactor, Mater. Today Proc. 4 (2017) 10118–10122. doi:10.1016/J.MATPR.2017.06.332.

[15] M. Mahdavi, M. Sharifpur, J.P. Meyer, CFD modelling of heat transfer and pressure drops for nanofluids through vertical tubes in laminar flow by Lagrangian and Eulerian approaches, Int. J. Heat Mass Transf. 88 (2015) 803–813. doi:10.1016/J.IJHEATMASSTRANSFER.2015.04.112.

[16] H. Ghodsinezhad, M. Sharifpur, J.P. Meyer, Experimental investigation on cavity flow natural convection of Al2O3–water nanofluids, Int. Commun. Heat Mass Transf. 76 (2016) 316–324. doi:10.1016/J.ICHEATMASSTRANSFER.2016.06.005.

[17] M. Sharifpur, N. Tshimanga, J.P. Meyer, O. Manca, Experimental investigation and model development for thermal conductivity of α-Al2O3-glycerol nanofluids, Int. Commun. Heat Mass Transf. 85 (2017) 12–22. doi:10.1016/J.ICHEATMASSTRANSFER.2017.04.001.

[18] M. Sharifpur, A.B. Solomon, T.L. Ottermann, J.P. Meyer, Optimum concentration of nanofluids for heat transfer enhancement under cavity flow natural convection with TiO2 – Water, Int. Commun. Heat Mass Transf. 98 (2018) 297–303. doi:10.1016/J.ICHEATMASSTRANSFER.2018.09.010.

[19] S. Osman, M. Sharifpur, J.P. Meyer, Experimental investigation of convection heat transfer in the transition flow regime of aluminium oxide-water nanofluids in a rectangular channel, Int. J. Heat Mass Transf. 133 (2019) 895–902. doi:10.1016/J.IJHEATMASSTRANSFER.2018.12.169.

[20] N.E. Todreas, M.S. Kazimi, Nuclear System II; Elements of Thermal Hydraulic Design, Taylor& Francis, 2001.

[21] B.C. Pak, Y.I. Cho, Hydridynamic and Heat Transfer Study of Dispersed Fluids with Submicron Metalic Oxide Particles, Exp. Heat Transf. 11 (1998) 151–170. doi:10.1080/08916159808946559.

[22] S.-K. Cheng, N.E. Todreas, Hydrodynamic models and correlations for bare and wire-wrapped hexagonal rod bundles — Bundle friction factors, subchannel friction factors and mixing parameters, Nucl. Eng. Des. 92 (1986) 227–251. doi:10.1016/0029-5493(86)90249-9.

[23] N.E. Todreas, M.S. Kazimi, Nuclear System I; Thermal Hydraulic Fundementals, Taylor & Francis, 1990.

[24] Y. Xuan, W. Roetzel, Conceptions for heat transfer correlation of nanofluids, Int. J. Heat Mass Transf. 43 (2000) 3701–3707. doi:10.1016/S0017-9310(99)00369-5.

[25] M.W. Chase, NIST-JANAF Thermochemical Tables, 4th Edition, J. Phys. Chem. Ref. Data, Monogr. 9. Monograph (1998) 1952. doi:citeulike-article-id:12140840.

[26] J.M. Doster, Assessment of the Performance of COBRA-TF for the Prediction of Subcooled Boiling Conditions in Rod Bundles, 2013.

[27] W. Yu, S.U.S. Choi, The Role of Interfacial Layers in the Enhanced Thermal Conductivity of Nanofluids: A Renovated Maxwell Model, J. Nanoparticle Res. 5 (2003) 167–171. doi:10.1023/A:1024438603801.

[28] G. Markoczy, Convective heat transfer in rod clusters with turbulent axial coolant flow. P. 1, Waerme Stoffuebertrag. 5 (1972) 204–212. https://inis.iaea.org/search/search.aspx?orig_q=RN:4066831 (accessed February 7, 2019).

[29] V. Gnielinsky, New equations for heat and mass transfer in turbulent pipe and channel flow, Int. Chem. Eng. 16 (1976) 359–368.

[30] R. Nourollahi, M.H. Esteki, G. Jahanfarnia, Thermal-hydraulic noise analysis of a VVER-1000 reactor with nanofluid as coolant, Prog. Nucl. Energy. 108 (2018) 334–350. doi:10.1016/j.pnucene.2018.06.010.

[31] S.J. Palandi, M. Rahimi-esbo, R. Mohammadyari, Numerical Simulation of Flow and Heat Transfer of, 4 (2014) 1448–1462.

[32] E. Zarifi, G. Jahanfarnia, Subchannel analysis of TiO2 nanofluid as the coolant in VVER-1000 reactor, Prog. Nucl. Energy. 73 (2014) 140–152. doi:10.1016/j.pnucene.2014.02.004.

[33] E. Zarifi, G. Jahanfarnia, F. Veysi, Subchannel analysis of nanofluids application to VVER-1000 reactor, Chem. Eng. Res. Des. 91 (2013) 625–632. doi:10.1016/j.cherd.2013.01.018.

[34] E. Zarifi, S. Tashakor, Subchannel analysis of Al2O3 nanofluid as a coolant in VMHWR, Kerntechnik. 80 (2015) 440–448. doi:10.3139/124.110542.

[35] Oak Ridge National Laboratory, COBRA-EN; Code System for Thaermal-Hydraulic Transient Analysis of Light Water Reactor Fuel assembelies and Cores, 2001.

[36] Jubair Ahmed, S., 2015. Numerics Applied Nanofluid Analysis in a Square Array Subchannel. Seoul National University. http://hdl.handle.net/10371/123496

Figure Captions: